ACS Sustainable Chemistry & Engineering

Research Article

pubs.acs.org/journal/ascecg

Effects of Microwave-Hydrothermal Conditions on the Purity and Electrochemical Performance of Orthorhombic $LiMnO_2$

Hongmei Ji, Xiaowei Miao, Lu Wang, Bing Qian,* and Gang Yang*

Jiangsu Laboratory of Advanced Functional Material, Changshu Institute of Technology, Changshu 215500, China

ABSTRACT: This paper reports the different reaction conditions to synthesize the orthorhombic $LiMnO_2$ (hereafter referred as *o*-$LiMnO_2$) and to find the economic usage of raw material to obtain the pure *o*-$LiMnO_2$ with ideal electrochemical performance via effective and energy-saving microwave-hydrothermal (MH) routine. The product formation mechanism in different process is discussed in detail. X-ray diffraction patterns (XRD) indicate that the MH temperature and time are more important than the LiOH concentration of the precursors to influence the phase purity of the products. The pure phased *o*-$LiMnO_2$ prepared under optimized MH condition exhibits the maximum discharge capacity of 228 mA h/g and reversible capacity of 160 mA h/g after 50 cycles at 0.1 C rate. When the current density increased to 0.2 and 0.5 C, the maximum discharge capacities of *o*-$LiMnO_2$ maintain at 197 and 165 mA h/g, respectively. The *o*-$LiMnO_2$ obtained in controlled MH condition shows the enhanced electrochemical performance compared with those synthesized by other method, indicating its potential application in the lithium-ion battery field.

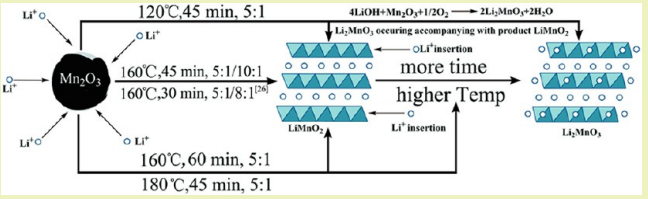

KEYWORDS: *Lithium ion batteries, Microwave-hydrothermal synthesis, o-$LiMnO_2$, Cathode material, Purity, Performance*

INTRODUCTION

Li-ion secondary batteries (LIB) are becoming the principal choice for power sources of portable electronic devices such as laptop computer, cellular phones, and so on.[1−4] $LiCoO_2$ is the primary cathode material of battery in the commercial applications because of its long cycle life and excellent discharge capacity. However, its remaining drawbacks such as high cost, environment toxicity, and safety problems have led to enormous interest in developing alternative cathode materials.[4−8]

Li−Mn−O compounds because of their low cost, numerous occurrence, and environmental acceptable characteristics have attracted great interests of many researchers. Among them spinel-type $LiMn_2O_4$ with a three-dimensional framework structure is considered as one of the prerequisites for electric vehicle based application due to its high rate capability.[9] Moreover, its poor cyclic performance is expected to improve and Aravindan et al. has synthesized porous $LiMn_2O_4$ hollow nanofibers retaining 87% of initial reversible capacity after 1250 cycles at the 1 C rate.[10] However, the specific capacity of the $LiMn_2O_4$ is 110−120 mA h/g, nearly one half of the capacity of the $LiMnO_2$, which has a high theoretical capacity of 285 mA h/g and was with great advantages for lithium-ion battery systems among the lithium manganese oxide.[11,12]

Current study on $LiMnO_2$ is mainly concentrated on orthorhombic phase because the monoclinic phase is considered very difficult to obtain.[13,14] In order to obtain *o*-$LiMnO_2$ with good capacity and cyclic behavior, different methods were employed to prepare that type $LiMnO_2$, such as those of conventional solid-state,[15−17] reverse microemulsion preparation,[18] and hydrothermal.[19−23] Detailed investigation on the electrochemical properties of *o*-$LiMnO_2$ cathode material showed that a conventional hydrothermal process is a good choice for synthesizing the *o*-$LiMnO_2$ particles with suitable size and good electrochemical performances.[19−25] For example, Qun et al. reported that the reaction conditions, such as reaction temperature and the concentration of the reactant, should be strictly controlled within a small range to synthesize the pure *o*-$LiMnO_2$ products in the hydrothermal process with good electrochemical performances.[21] Changing the conventional heating style to microwave irradiation in the hydrothermal process, it forms an improved route as microwave-hydrothermal (MH), which was experimented on synthesizing *o*-$LiMnO_2$ with desired results in our preliminary work.[26] Recently, Li et al. has been used MH method to synthesize other manganese oxide as electrode candidate for supercapacitor.[27]

On the basis of the presynthesizing work, further experiments in this work have been done to investigate the influence of the reaction conditions on the product phases and electrochemical performance of the products. The sample *o*-$LiMnO_2$ with the best electrochemical properties has been synthesized in optimized MH condition.

EXPERIMENTAL SECTION

The typical process for synthesizing the sample *o*-$LiMnO_2$ is described as follows. A 0.0075 mol portion of α-Mn_2O_3 (obtained by the calcination of $MnCO_3$ at 700 °C for 3 h in air) was added into 40 mL distilled water, with a continuous stirring for 5 min. A 0.075 mol portin

Received: March 28, 2013
Revised: November 18, 2013
Published: November 27, 2013

of $LiOH{\cdot}H_2O$ was added into the suspension. The mixed solution was stirred for 24 h before transferred into a 70 mL polytetrafluoroethene (PTFE) vessel. MH treatment was performed in the Shanghai Sineo microwave digestion system (MDS-6) under 160 °C for 45 min to produce *o*-$LiMnO_2$. When the vessel was cooled down, a dark brown precipitate was collected and washed with distilled water for several times and finally dried in a vacuum oven at 60 °C for 20 h. For comparison, various sets of MH reaction parameters, the Li/Mn molar ratio ($C_{Mn^{2+}}$ = 0.375 mol/L), microwave irradiation time, and temperature, were attempted and listed in Table 1. The products are

Table 1. List of Obtained Samples in Different Conditions

name of compound	time (min)	temperature (°C)	Li/Mn
MH160_2r1_45m	45	160	2:1
MH160_5r1_45m	45	160	5:1
MH160_10r1_45m	45	160	10:1
MH160_5r1_30m	30	160	5:1
MH160_5r1_60m	60	160	5:1
MH120_5r1_45m	45	120	5:1
MH180_5r1_45m	45	180	5:1

named MH 160_5r1_45m (MH is the abbreviation of microwave-hydrothermal, 160 means the MH temperature of 160 °C, 5r1 means the precursors of Li:Mn = 5:1, 45m means MH time for 45 min). The following abbreviations are identical.

The products were characterized by X-ray diffraction (XRD) in reflection mode (Cu Kα radiation) on a Rigaku D/max-2200/PC diffractometer in the 2θ range from 10 to 70°. The morphologies were observed with the JEOL6700 field-emission scanning electron microscope.

Electrochemical measurements were carried out with coin cell. The working electrodes were prepared by mixing the obtained *o*-$LiMnO_2$, acetylene black, and polytetrafluoroethylene (PTFE) in the weight ratio of 80:15:5. Cells were assembled in an argon filled glovebox using Celgard 2300 membrane as a separator, a solution of 1 mol/L $LiPF_6$ in ethylene carbonate (EC)/ dimethyl carbonate (DMC) (1:1 ratio in weight) as the electrolyte. The galvanostatic charge and discharge cycling was studied in the voltage range of 2.0−4.4 V at different current densities by LAND CT2001A battery testing system (Wuhan, China).

RESULTS AND DISCUSSION

Phase Transition and Morphological Evolution during the Formation of *o*-$LiMnO_2$. Figure 1 shows the XRD patterns of the reagent α-Mn_2O_3 and the obtained *o*-$LiMnO_2$ sample MH160_5r1_45m with their indexing results. The XRD patterns of α-Mn_2O_3 decomposed by $MnCO_3$ at 700 °C for 3 h in air is shown in Figure 1a, and all of the reflection peaks can

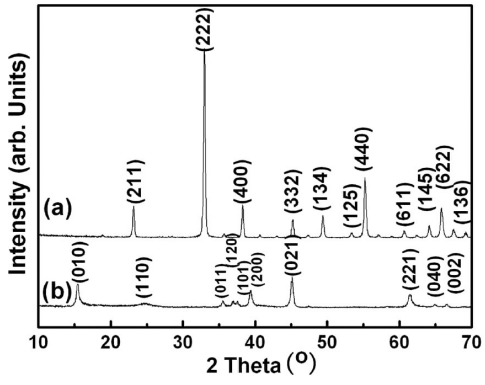

Figure 1. XRD patterns of the (a) α-Mn_2O_3 precursor and the (b) *o*-$LiMnO_2$ product.

be indexed with cubic structure for α-Mn_2O_3 (JCPDS card 78-0390). After the mixture of α-Mn_2O_3 and LiOH treated in the microwave-hydrothermal system, a new XRD pattern of the product quite different from that of α-Mn_2O_3 is shown in Figure 1b. According to the JCPDS card 35-0749, the peaks of the new phase labeled in Figure 1b can be indexed as orthorhombic phase of $LiMnO_2$ with a space group of *Pmmn*. Compared with other methods assisting by traditional heating style reported previously 28−35, MH routine showed a great decrease in the required reaction time to produce the pure *o*-$LiMnO_2$.

The SEM and TEM images presented in Figure 2 exhibit both the starting material α-Mn_2O_3 and the as-obtained pure *o*-$LiMnO_2$. Figure 2a shows that α-Mn_2O_3 micrometer powders possess the irregular shape with smooth margin. The morphology observed from TEM image (Figure 2c) shows that the irregular nanospheres are secondary structure combined with small particles. The SEM image of the as-obtained *o*-$LiMnO_2$ in Figure 2b exhibits powders that are accumulated with the cube particles of apparent edges. The cube particles can be seen in Figure 2d, and their sizes are 50−100 nm, smaller than the raw material α-Mn_2O_3. High magnification of the image (Figure 2d inset) indicates that the lattice fringe of the product is 0.57 nm corresponding to (010) plane of *o*-$LiMnO_2$. The morphology changes imply that the crystal growth included the dissolution of α-Mn_2O_3 to form coordination polyhedron of $[Mn(OH)_6]^{3-}$ and then incorporated by Li^+ to form *o*-$LiMnO_2$.[33] α-Mn_2O_3 dissolves in LiOH under high alkali environment to grow an intermediate before obtaining the product, which also has been proved by He et al. to synthesize $LiMn_{1-x}Al_xO_2$.[33] LiOH supplies a basic corrosive environment to accelerate the α-Mn_2O_3 spheres to dissolve and to grow the new precipitation of *o*-$LiMnO_2$ with cube morphology. LiOH not only provided the Li ions for the formation of *o*-$LiMnO_2$ but also assumed the task of changing the morphology and reducing the grain size by its basic corrosive characteristics.[21]

Influence of Microwave-Hydrothermal Parameters on the Phase Purity of the Product. *o*-$LiMnO_2$ has been successfully synthesized via the rapid microwave-hydrothermal route in our previous work.[26]To prepare the product with pure phase and optimal electrochemical performance, various parameters were attempted in the present experiments. The factors of ratio between LiOH and α-Mn_2O_3, MH temperature, and MH time would most likely influence the purity of the product. The theoretically ratio 2:1 between the raw materials (LiOH: α-Mn_2O_3) was thought to be necessary for *o*-$LiMnO_2$ formation and the using amount of LiOH should be relatively economical. As for the factor of ratio between LiOH and α-Mn_2O_3, the ratio was controlled between 2:1 and 10:1 in the present work.

XRD patterns in Figure 3 show the effects of LiOH concentration on the purity of obtained products, on which (Figure 3c) the theoretical amount of 0.030 mol LiOH (Li/Mn = 2:1) was not enough to react with the total α-Mn_2O_3 to produce the aimed *o*-$LiMnO_2$. The final products MH160_2r1_45m contained mainly raw material α-Mn_2O_3 labeled with circle, as well as only a small amount of *o*-$LiMnO_2$ indicated by square. This problem could be solved by increasing the amount of LiOH, which has been proved by the XRD patterns of the products MH160_5r1_45m and MH160_10r1_45m in Figure 3a and b. Pure phase *o*-$LiMnO_2$ products were obtained under the condition of

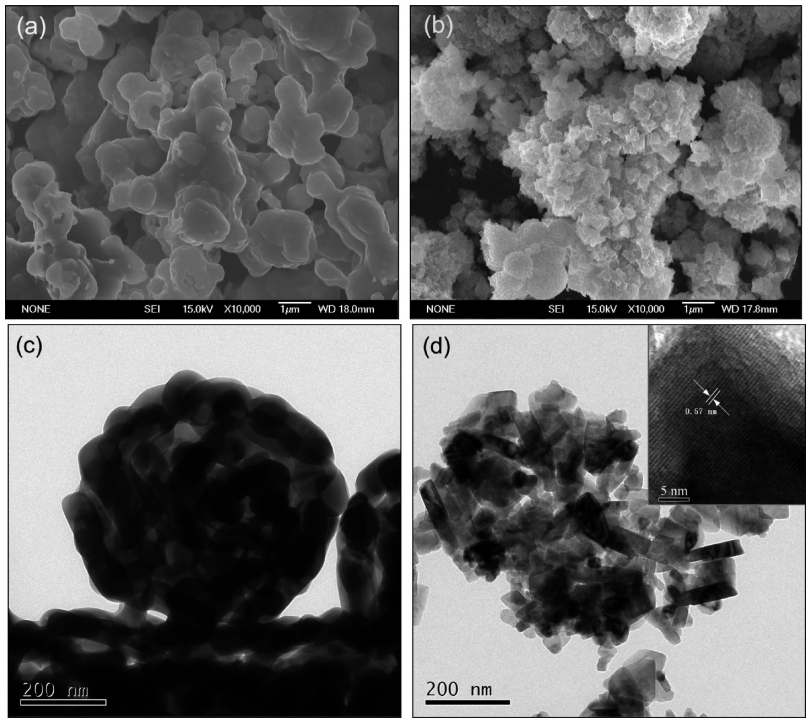

Figure 2. SEM and TEM images of (a and c) α-Mn_2O_3 precursor and (b and d) the pure-phased o-$LiMnO_2$ product.

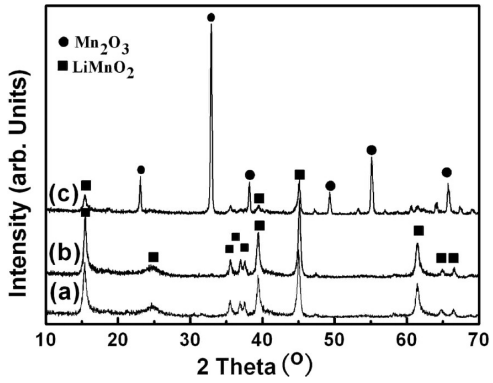

Figure 3. XRD patterns of the obtained products of (a) MH160_10r1_45m, (b) MH160_5r1_45m, and (c) MH160_2r1_45m.

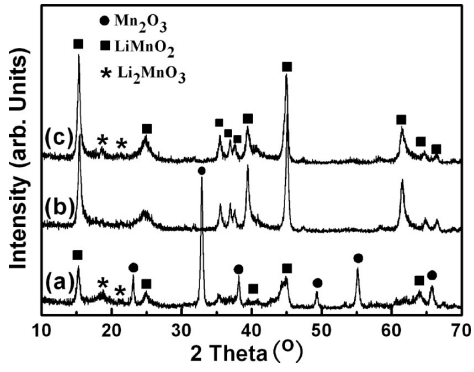

Figure 4. XRD patterns of the obtained products of (a) MH120_5r1_45m, (b) MH160_5r1_45m, and (c) MH180_5r1_45m.

LiOH:Mn_2O_3= 5:1 and 10:1, respectively. It indicates that the ratio between LiOH and α-Mn_2O_3 had the effect on the phase purity of the final product. The solution with enough alkaline was benefit for the α-Mn_2O_3 to dissolve into $[Mn(OH)_6]^{3-}$, and high concentration of Li ions could increase its mobility and reactivity with Mn source.[35]

In the experiment, MH temperature was also very important in the formation of pure phase o-$LiMnO_2$. The XRD results of the samples obtained in different temperatures are shown in Figure 4. It could be seen that the main phase of the product MH120_5r1_45m was α-Mn_2O_3 besides a little o-$LiMnO_2$ and Li_2MnO_3 labeled with square and asterisk, respectively. When the MH temperature increased to 160 °C, the α-Mn_2O_3 phase disappeared and the crystalline phase o-$LiMnO_2$ occurred in the product MH160_5r1_45m as shown in Figure 4b. Nevertheless, in the MH process the slightly changing of the temperature would influence the purity of the products due to its special and rapid heating mechanism and other metastable phases Li−Mn−O compounds existing. When the temperature further increased to 180 °C, another Li−Mn−O compound, called Li_2MnO_3 appeared as shown in Figure 4c. The above results suggested that the suitable MH temperature was a key factor for obtaining the pure phase o-$LiMnO_2$.

MH treating time also has great effect on the purity of the final products. Upon microwave irradiation up to 60 min, the Li_2MnO_3 would come to appear, as shown in the product MH160_5r1_60m (Figure 5a). XRD patterns of Figure 5b and c show that the products MH160_5r1_30m and MH160_5r1_45m are purity without apparent Li_2MnO_3, which indicates that relatively short microwave irradiation time is more suitable for synthesizing pure phase of o-$LiMnO_2$. The experiment results on the above three aspects show that the MH treating parameters are still limited to be employed for preparing pure phase o-$LiMnO_2$ in similar to what being controlled in traditional hydrothermal. On the basis of the analysis of above XRD results, detailed products formation

dx.doi.org/10.1021/sc400439k | ACS Sustainable Chem. Eng. 2014, 2, 359−366

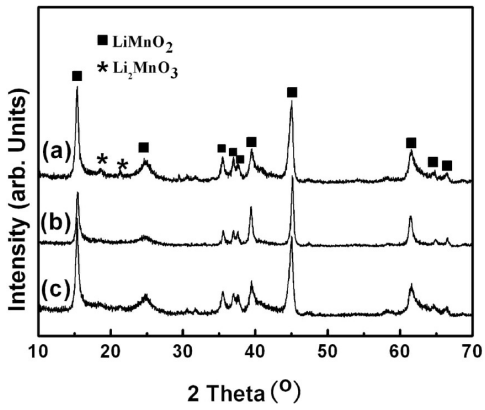

Figure 5. XRD patterns of the obtained products of (a) MH160_5r1_60m, (b) MH160_5r1_45m, and (c) MH160_5r1_30m.

mechanism in the different reaction time and temperature was present as follows.

Figure 6 shows the schematic of the product formation mechanism in different process including the product MH 160_8r1_30m referred in our last paper.[26] It could be shown that Li_2MnO_3 occurred accompanying with the aimed product *o*-$LiMnO_2$ at the low temperature 120 °C, which was accordance with the theory that has reported by Jang et al.[29] It proved that when the oxygen was at a certain quantity in the autoclave, the oxidation reaction was accelerated at the low temperature as follows: $4LiOH + Mn_2O_3 + {}^1/_2O_2 = 2Li_2MnO_3 + 2H_2O$.[36] Lower temperature was benefit for the direct oxidation of α-Mn_2O_3 to Li_2MnO_3 at 120 °C in this work. Compared with the product MH 160_5r1_45m, minor Li_2MnO_3 appeared in the MH 160_5r1_60m and MH 180_5r1_45m, which is attributed to the more heating time and higher temperature in the synthesizing process, respectively. In relatively high temperature, Mn ion preferred to be in the reduction state.[36] Li ion first reacts with Mn source to form *o*-$LiMnO_2$ such as in the process of synthesizing product MH 160_5r1_45m, the idealized structure of which was with layer structure comprised by Li^+ layer and MnO_6 octahedra layer.[37] More time and high temperature accelerate the monovalent lithium to migrate to the MnO_6 octahedra layer to form the Li_2MnO_3 ($Li[Li_{1/3}Mn_{2/3}]O_2$), in which tetravalent manganese and monovalent lithium comprise the MnO_6 octahedra layer.[37] According to the above comparative analysis of the results of the different processes, the key factors to synthesize the pure product are the reaction time and temperature, but not the ratio between Li and Mn. It could be seen that the Li/Mn (5:1, 8:1, 10:1) is all suitable for obtaining in the condition of suitable temperature and reaction time. This mechanism would be a guide for preparing pure-phased *o*-$LiMnO_2$ for further investigation or application.

Electrochemical Performance. On the basis of successful obtaining the different products prepared in the different microwave hydrothermal conditions, further investigation on electrochemical performance of the whole obtained products was made to find out the optimized MH parameters.

Figure 7a shows the charge/discharge curves of the cycles with the maximum discharge capacity for the samples of MH 160_2r1_45m, MH 160_5r1_45m, and MH 160_10r1_45m, respectively, and Figure 7b shows their cyclic performances. It can be seen that the product MH160_2r1_45m achieved the maximum discharge capacity of 79 mA h/g and much lower than those of the other two products MH 160_5r1_45m and MH 160_10r1_45m. It was caused by the existence of large proportion of raw material α-Mn_2O_3 in the final product MH160_2r1_45m as proved by XRD pattern of Figure 3c. In regard to the pure *o*-$LiMnO_2$ products of MH 160_5r1_45m and MH 160_10r1_45m obtained in the relatively high alkaline environment, both of the products are with the same maximum capacity 228 mA h/g. However, there are still some distinctions such as the capacity of the discharge plateau (in Figure 7a), the cyclic performance, and the discharge capacity for the first cycle (as seen in Figure 7b).

Previous research suggested that the distinct discharge voltage plateaus around 4 and 3 V were the indicative of Li intercalation on different sites, tetrahedral site over 4 V, and octahedral site over 3 V in the cycling-induced spinel $LiMn_2O_4$.[38] As shown in Figure 7a, the capacity near the 4 V discharge profile plateau in MH160_5r1_45m is bigger than that of the product MH160_10r1_45m, while that of the 3 V plateau is small in the product MH160_5r1_45m. Therefore, the Li intercalation in that product on the tetrahedral site over 4 V was more and on the octahedral site over 3 V in the cycling-induced spinel $LiMn_2O_4$ was less compared with that in the product MH160_10r1_45m.

Figure 8a and b show the discharge curves and the differential discharge capacity plots for typical cycles inserted for MH160_5r1_45m and MH160_10r1_45m, respectively. The product MH160_5r1_45m reaches the maximum discharge capacity 228 mA h/g at the seventh cycle, in which cycle the capacity of 3 V plateau as the Li intercalation on the octahedral site became the biggest among all discharge cycles (as shown in Figure 8a). The 4 V plateau is divided into two subplateaus because of the reordering of Li in the structure, and the peak splitting of differential discharge plots around the 4 V plateau of the 1st, 7th, and 20th became more and more large as exhibited in Figure 8a (inset). It would be beneficial to increase the discharge capacity of the *o*-$LiMnO_2$ and compensate the capacity fading gradually around 3 V plateau

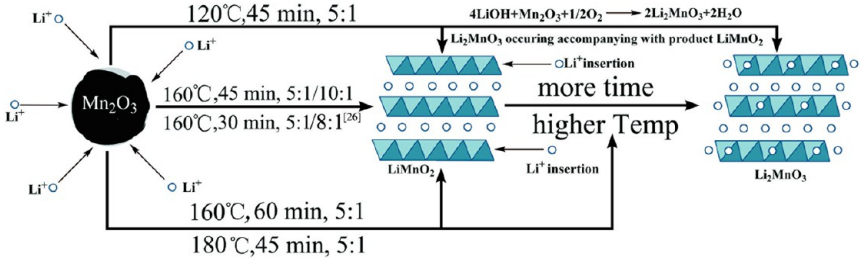

Figure 6. Schematic of the product formation mechanism in different process.

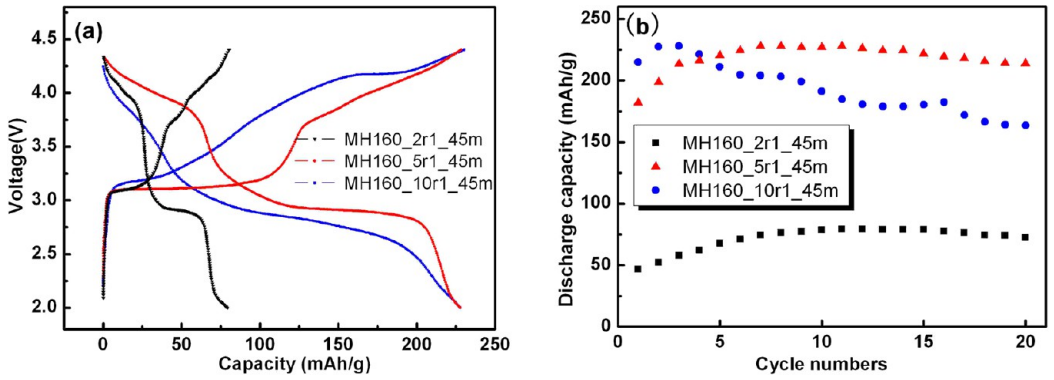

Figure 7. (a) Charge/discharge profiles of the cycle with the maximum discharge capacity and (b) cyclic performance of the samples obtained with different ratio between LiOH and α-Mn_2O_3.

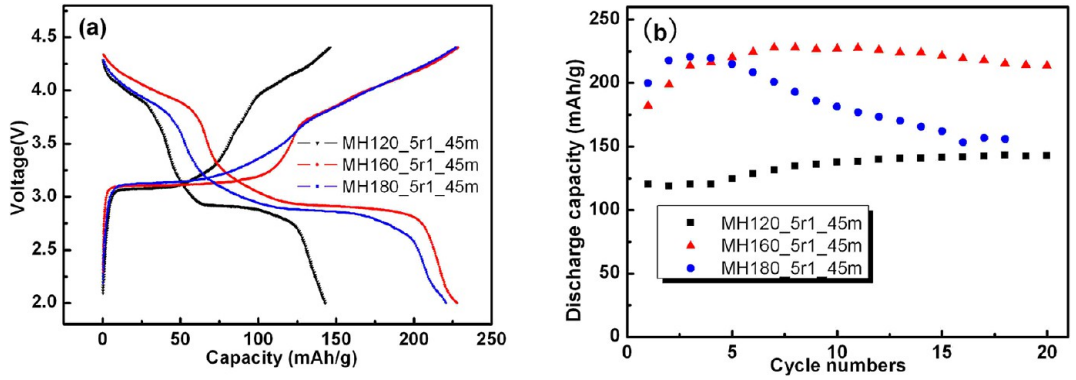

Figure 8. Discharge plots and the differential discharge capacity plots on cycling for typical cycles (in inset) for (a)MH 160_5r1_45m and (b) MH 160_10r1_45m.

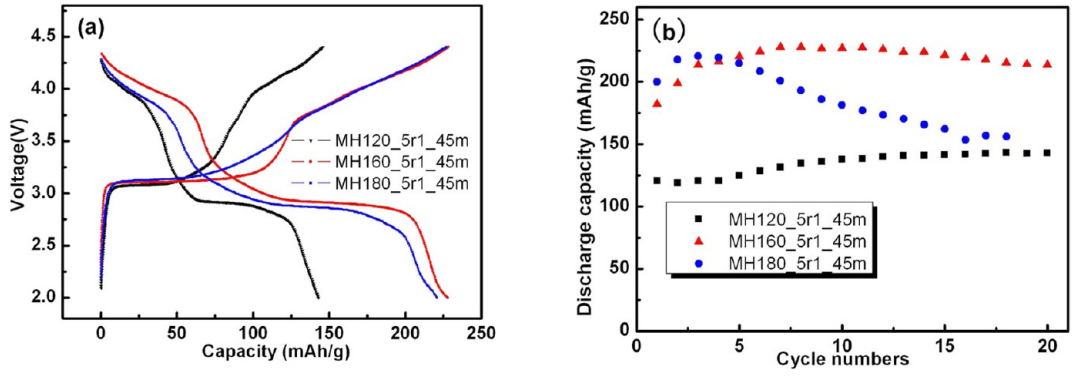

Figure 9. (a) Charge/discharge profiles of the cycle with the maximum discharge capacity and (b) cyclic performance of the samples obtained with different reaction temperature.

to maintain the high discharge capacity. The product MH160_5r1_45m was with good cyclic performance and remained discharge capacity of 214 mA h/g after 20 cycles.

Compared with MH160_5r1_45m, the product MH160_10r1_45m was with less Li intercalation on the tetrahedral site and the reordering of Li in the structure on cycling did not happen apparently because of no splitting of the peaks around the 4 V (as shown in Figure 8b inserted). This made the capacity from the 4 V plateau without enough increasing to defense the capacity fading at the 3 V plateau. Therefore, the discharge capacity of this product faded fast and only 164 mA h/g discharge capacity was kept for only 20 cycles. The product MH160_10r1_45m reaches to the highest discharge capacity in third cycle. It might be due to the fact that the phase transformation of *o*-$LiMnO_2$ from orthorhombic to cycling-induced spinel with the Li intercalation on the octahedral site developed much faster and more complete in the initial charge/discharge stage.

The electrochemical tests were also made for the samples obtained in different temperature, and their charge/discharge curves of the cycles with the maximum discharge capacity and cyclic performances are shown in Figure 9a and b, respectively. The maximum discharge capacity of MH 120_5r1_45m only 143 mA h/g (as shown in Figure 9b) is the smallest among the three samples, due to the impurity Mn_2O_3 present in the sample. The maximum discharge capacities of MH 160_5r1_45m and MH 180_5r1_45m were 228 and 221 mAh/g, respectively. Figure 9b also shows that MH

dx.doi.org/10.1021/sc400439k | ACS Sustainable Chem. Eng. 2014, 2, 359−366

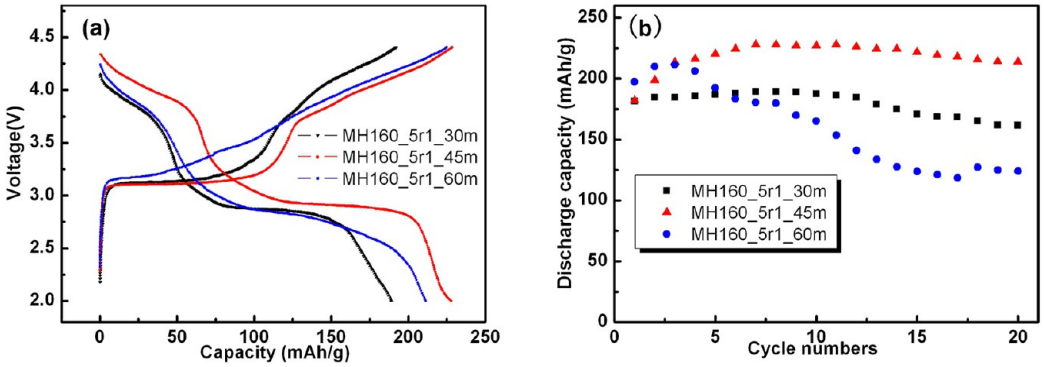

Figure 10. (a) Charge/discharge profiles of the cycle with the maximum discharge capacity and (b) cyclic performance of the samples obtained with different reaction time.

180_5r1_45m reaches the maximum discharge capacity faster than that of the MH 160_5r1_45m. But the capacity-fading tendency of the MH 180_5r1_45m is much higher than MH 160_5r1_45m, which may be caused by the formation of Li_2MnO_3 in the MH process. It has been reported that Li_2MnO_3 obtained in hydrothermal condition was with high initial discharge capacity but fading fast.[39]

The MH time also plays an important role in the electrochemical performance of the obtained products and their typical electrochemical performances are shown in Figure 10a and b. The product MH 160_5r1_30m and MH 160_5r1_45m attained the maximum capacity nearly at the same cycle, which could further prove that both of the two products were pure-phased *o*-$LiMnO_2$. The discharge capacity of MH 160_5r1_45m and cyclic performance are better than those of MH 160_5r1_30m because of the different crystal quality of the two products obtained at different MH time. As for the product MH 160_5r1_60m with a little impurity Li_2MnO_3, it exhibited the similar initial capacities with MH 180_5r1_45m. It had high first discharge capacity 211 mAh/g and reached its maximum discharge capacity at the third cycle as shown in Figure 10a and b, the same cycle with that of MH 180_5r1_45m. In addition, its capacity decreased dramatically because of the existence of Li_2MnO_3 and made 88 mA h/g capacity loss during 20 cycles (as shown in Figure 10b).

The above results and discussion of the electrochemical performances for the whole products obtained in different MH conditions suggested that the product MH160_5r1_45m exhibited the best capacity and cyclic performance. Figure 11 shows the cyclic performances of MH160_5r1_45m at different current rate (0.1, 0.2, and 0.5 C). The product MH 160_5r1_45m cycled at 0.1 C has the maximum discharge capacity of 228 mA h/g and remained 208 and 160 mA h/g at the 30th and 50th, respectively. From Figure 11, it also could be seen that the maximum discharge capacity of this product remained at 197 and 165 mA h/g at 0.2 and 0.5 C, respectively. When the current rate was 0.2 C, the discharge capacity faded slowly before the 30th cycle (162 mA h/g). Concerning the current rate at 0.5 C, the capacity of the product was relative low, with the maximum discharge capacity of 164 mA h/g and remaining 114 mA h/g until the 50th cycle.

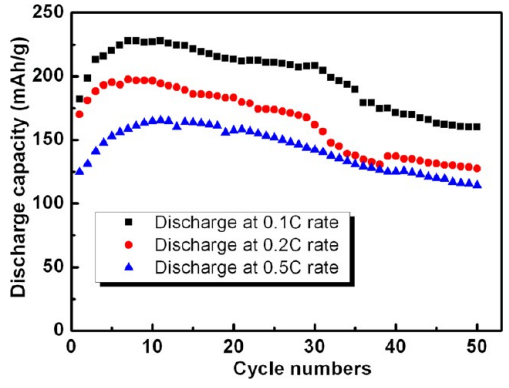

Figure 11. Cyclic performance of MH 160_5r1_45m at 0.1, 0.2, and 0.5 C.

Comparing with the data obtained for $LiMnO_2$ synthesized with different methods (as shown in Table 2), it could be seen that microwave hydrothermal is an ideal route to synthesize *o*-$LiMnO_2$ with good electrochemical performance. Using this method, the pure *o*-$LiMnO_2$ can be obtained in a very short time and low temperature, and the discharge capacity of the product is higher than those reported nowadays expect the $Li_{0.99}Mn_{0.988}In_{0.012}O_{1.991}S_{0.009}$ doped with In and S.[30] Besides, the product obtained in this work has a satisfactory discharge capacity in relative high current density 0.2 and 0.5 C, and few papers reported the electrochemical performance data under different current rates.[34,35] Through adjusting the reaction conditions, the capacity and cyclic performance of the product MH 160_5r1_45m was also improved comparing with the last reported product obtained at 160 °C for 45 min with the Li:Mn = 8:1. Moreover, it is not hard to find that the consumption of LiOH was nearly 40% lower than the reported data 26, and it can still obtain the pure *o*-$LiMnO_2$ with even more improved electrochemical performance. With the widespread use of lithium ion batteries, the lithium resource is increasingly scarce, and He et al. published a paper specializing in how to lower the mole ratio of Li/Mn,[35] so it is of great significance to increase the use ratio of Li using this microwave-hydrothermal method.

CONCLUSIONS

The microwave-hydrothermal conditions were detailed discussed to prepare the *o*-$LiMnO_2$ and suitable conditions for obtaining the pure products were completely understood. The purity of the *o*-$LiMnO_2$ was sensitive to the reaction temperature and time. The ratio between LiOH and α-Mn_2O_3 could be decreased from 10:1 to 5:1. The sample MH 160_5r1_45m synthesized in optimized MH condition has the high capacity and good cyclical performance, with maximum discharge capacity of 228 mA h/g, remaining the capacity of 208 mA h/g after 30 cycles at 0.1 C. When the current density increased to 0.2 and 0.5 C, the maximum discharge capacity still

Table 2. Data Obtained for $LiMnO_2$ Synthesized with Different Methods

product	method	charge/discharge voltage range	temperature/time	current density	first/maximum/other cycle discharge capcacity (mA h/g)	ref
$LiMnO_2$	solid-state	2.0−4.3 V	900 °C/12 h	C/7	25/120/120(30th)	28
$LiMnO_2$	hydrothermal	2.0−4.5 V	160 °C/12 h	C/10	172/173/162(20th)	21
$LiMnO_2$	hydrothermal	2.0−4.5 V	180 °C/24 h	C/10	148/260/245(30th)	22
$LiMnO_2$	solid-state	2.0−4.4 V	700 °C/5 h	C/19	90.2/152/125(50th)/114(80th)	29
$Li_{0.99}Mn_{0.988}In_{0.012}O_{1.991}S_{0.009}$	hydrothermal	2.0−4.3 V	150 °C/36 h	C/5.7	108/267.9/256(60th)	30
$LiMnO_2$	hydrothermal	2.0−4.5 V	200 °C/2−4 h	C/28.5	235/235/190(20th)	31
$LiMn_{0.9}Cr_{0.1}O_2$	solution-assisted solid-state	2.5−4.5 V	90-180-300 °C/6h-600 °C/ 4h -800 °C/15 h	C/10	210/210/200(30th)	32
$LiMn_{1-x}Al_xO_2$	hydrothermal	2.0−4.3 V	150 °C/12−72 h	C/10	175/190/145(25th)	33
$LiMnO_2$−Li_2MnO_3	hydrothermal	2.0−4.5 V	200 °C/72 h	C/28.5	180/192/182(5th)	34
				C/5.7	134.4(6th)/136/125(10th)	
				C/2.8	95(11th)/95/95(5th)	
$LiMnO_2$	solvothermal	2.0−4.2 V	170 °C/72 h	C/20	166/170/150(6th)	35
				C/10	132(7th)/132/130(12th)	
				C/5	98(13th)/98/98(18th)	
$LiMnO_2$	microwave-hydrothermal	2.2−4.4 V	160 °C/30 min Li:Mn= 8:1	C/10	176/194/184(20th)	26
$LiMnO_2$	microwave-hydrothermal	2.0−4.2 V	160 °C/45 min Li:Mn = 5:1	C/10	182/228/208(30th)/160(50th)	this work
				C/5	170/194/162(30th)/128(50th)	
				C/2	125/165/142(30th)/114(50th)	

maintained at 197 and 165 mA h/g, respectively. The discharge capacity at 0.2 C faded slowly and remained 162 mA h/g at the 30th cycle. Such results in different current rate confirmed the positive role of microwave hydrothermal on synthesizing the *o*-$LiMnO_2$ with good electrochemical performance, but we still should develop other additional ways such as doping other metals, coating C in this system for further improving its cyclic ability especially after dozens of cycle.

AUTHOR INFORMATION

Corresponding Authors

*Tel: 86-512-52251898. Fax: 86-512-52251842. E-mail: gyang@cslg.edu.cn
*E-mail: njqb@cslg.cn.

Notes

The authors declare no competing financial interest.

ACKNOWLEDGMENTS

The work was supported by NSF of Jiangsu Educational Department of China (Grant No. 10KJA480001) and NSF of China (Grant No. 51172032, 11174043).

REFERENCES

(1) Whittingham, M. S. Lithium batteries and cathode materials. *Chem. Rev.* **2004**, *104*, 4271−4301.
(2) Liu, Q.; Mao, Q.; Chang, C. Phase conversion and morphology evolution during hydrothermal preparation of orthorhombic $LiMnO_2$ nanorods for lithium ion battery application. *J. Power Sources* **2007**, *173*, 538−544.
(3) Armand, M.; Tarascon, J. M. Building better batteries. *Nature* **2008**, *451*, 652−657.
(4) Ritchie, A. G. Preparation of α-Fe_2O_3 on stainless steel as anodes for Li-ion thin film battery by electrochemical method. *J. Power Sources* **2004**, *136*, 285−289.
(5) Choi, S.; Manthiram, A. Factors influencing the layered to spinel-like phase transition in layered oxide cathodes. *J. Electrochem. Soc.* **2002**, *149* (9), A1157−A1163.
(6) Baehtz, C.; Buhrmester, T.; Bramnik, N. N. Design and performance of an electrochemical in-situ cell for high resolution full-pattern X-ray powder diffraction. *Solid State Ionics* **2005**, *176*, 1647−1652.
(7) Goodenough, J. B; Mathiram, A.; Wnetrzewski, B. Effect of pH value on electrochemical property of tin/graphite composite anode materials by electroless plating method. *J. Power Source* **1999**, *343*, 269−275.
(8) Koksbang, R.; Barker, J.; Shi, H.; Saidi, M. Y. Cathode materials for lithium rocking chair batteries. *Solid State Ionics* **1996**, *84*, 1−21.
(9) Aravindan, V.; Gnanaraj, J.; Lee, Y. S; Madhavi, S. $LiMnPO_4$−A next generation cathode material for lithium-ion batteries. *J. Mater. Chem. A* **2013**, *1*, 3518.
(10) Jayaraman, S.; Aravindan, V.; Kumar, P. S; Ling, W. C; Ramakrishna, S.; Madhavi, S. Synthesis of porous $LiMn_2O_4$ hollow nanofibers by electrospinning with extraordinary lithium storage properties. *Chem. Commun.* **2013**, *49*, 6677.
(11) Jiang, Y.; Huang, B. Y; Wang, H. F; Sadoway, D. R; Chiang, Y. M. Electrochemical cycling-induced spinel formation in high-charge-capacity orthorhombic $LiMnO_2$. *J. Electrochem. Soc.* **1999**, *146* (9), 3217−3223.
(12) Wang, Q. S; Sun, J. H; Chen, C. H. Thermal stability of delithiated $LiMn_2O_4$ with electrolyte for lithium-ion batteries. *J. Electrochem. Soc.* **2007**, *154* (4), A263−A267.
(13) Tabuchi, M.; Ado, K.; Kobayashi, H.; Kageyama, H.; Masquelier, C.; Kondo, A.; Kanno, R. Synthesis of $LiMnO_2$ with α-$NaMnO_2$-type structure by a mixed-alkaline hydrothermal reaction. *J. Electrochem. Soc.* **1998**, *145* (4), L49−L52.
(14) Capitaine, F.; Gravereau, P.; Delmas, C. A new variety of $LiMnO_2$ with a layered structure. *Solid State Ionic* **1996**, *89*, 197−202.
(15) Bruce, P. G. Solid-state chemistry of lithium power sources. *Chem. Commun.* **1997**, 1817−1824.
(16) Thackeray, M. M. Manganese oxides for lithium batteries. *Prog. Solid State Chem.* **1997**, *25*, 1−71.
(17) Chitrakar, R.; Sakane, K.; Umeno, A.; Kasaishi, S.; Takagi, N.; Ooi, K. Synthesis of orthorhombic $LiMnO_2$ by solid-phase reaction under steam atmosphere and a study of its heat and acid-treated phases. *J. Solid State Chem.* **2002**, *169*, 66−74.
(18) Paulsen, J. M.; Thomas, C. L.; Dahn, J. R. Layered Li-Mn-oxide with the O_2 structure: a cathode material for Li-ion cells which does not convert to spinel. *J. Electrochem. Soc.* **1999**, *146* (10), 3560−3565.
(19) Lu, C. H.; Wang, H. C. Reverse-microemulsion preparation and characterization of ultrafine orthorhombic $LiMnO_2$ powders for lithium-ion secondary batteries. *J. Eur. Ceram. Soc.* **2004**, *24*, 717−723.

(20) Wu, M. Q.; Zhang, Q. Y.; Lu, H. P.; Chen, A. Nanocrystalline orthorhombic $LiMnO_2$ cathode materials synthesized by a two-step liquid-phase thermal process. *Solid State Ionics* **2004**, *169*, 47−50.
(21) Liu, Q.; Li, Y. X.; Hu, Z. L.; Chang, C. K.; Huang, F. Q. One-step hydrothermal routine for pure-phased orthorhombic $LiMnO_2$ for Li ion battery application. *Electrochim. Acta* **2008**, *53*, 7298−7302.
(22) Zhou, F.; Zhao, X. M.; Liu, Y. Q.; Li, L.; Yuan, C. G. Size-controlled hydrothermal synthesis and electrochemical behavior of orthorhombic $LiMnO_2$ nanorods. *J. Phys. Chem. Solids* **2008**, *69*, 2061−2065.
(23) Myung, S. T.; Komaba, S.; Kumagai, N. Hydrothermal synthesis and electrochemical behavior of orthorhombic $LiMnO_2$. *Electrochim. Acta* **2002**, *47*, 3287−3295.
(24) Myung, S. T.; Komaba, S.; Kumagai, N. Hydrothermal Synthesis of Orthorhombic $LiCo_xMn_{1-x}O_2$ and their structural changes during cycling. *J. Electrochem. Soc.* **2002**, *149* (10), A1349−A1357.
(25) Feng, Q.; Higashimoto, Y.; Kajiyoshi, K.; Yanagisawa, K. Synthesis of lithium manganese oxides from layered manganese oxides by hydrothermal soft chemical process. *J. Mater. Sci. Lett.* **2001**, *20*, 269−271.
(26) Ji, H. M.; Yang, G.; Miao, X. W.; Hong, A. Q. Efficient microwave hydrothermal synthesis of nanocrystalline orthorhombic $LiMnO_2$ cathodes for lithium batteries. *Electrochem. Acta* **2010**, *55*, 3392−3397.
(27) Li, L.; Seng, K. H.; Liu, H. K.; Nevirkovets, I. P.; Guo, Z. P. Synthesis of Mn_3O_4-anchored graphene sheet nanocomposites via a facile, fast microwave hydrothermal method and their supercapacitive behavior. *Electrochem. Acta* **2013**, *87*, 801−808.
(28) Wei, Y. J.; Ehrenberg, H.; Bramnik, N. N.; Nikolowski, K.; Baehtz, C.; Fuess, H. In situ synchrotron diffraction study of high temperature prepared orthorhombic $LiMnO_2$. *Solid State Ionics* **2007**, *178*, 253−257.
(29) Fan, G. X.; Zeng, Y. W.; Chen, R. S.; Lü, G. L Microstructure and electrochemical characterization of spherical-like orthorhombic $LiMnO_2$ via co-precipitation. *J. Alloys Compd.* **2008**, *461*, 267−272.
(30) Su, Z.; Lu, Z. W.; Gao, X. P.; Shen, P. W.; Liu, X. J.; Wang, J. Q. Preparation and electrochemical properties of indium- and sulfur-doped $LiMnO_2$ with orthorhombic structure as cathode materials. *J. Power Sources* **2009**, *189*, 411−415.
(31) He, Y.; Li, R. H.; Ding, X. K.; Jiang, L. L.; Wei, M. D. Hydrothermal synthesis and electrochemical properties of orthorhombic $LiMnO_2$ nanoplates. *J. Alloys Compd.* **2010**, *492*, 601−604.
(32) Pang, W. K.; Lee, J. Y.; Wei, Y. S.; Wu, S. H. Preparation and characterization of Cr-doped $LiMnO_2$ cathode materials by Pechini's method for lithium ion batteries. *Mater. Chem. Phys.* **2013**, *139*, 241−246.
(33) He, Y.; Yuan, F. M.; Ma, H.; Bai, X. D.; Yang, X. J. Influence of Al ions on the morphology and structure of layered $LiMn_{1-x}Al_xO_2$ cathode materials for the lithium ion battery. *J. Alloys Compd.* **2013**, *569*, 67−75.
(34) Dang, F.; Hoshino, T.; Oaki, Y. Y.; Hosono, E. J.; Zhou, H. S.; Imai, H. Synthesis of Li-Mn-O mesocrystals with controlled crystal phases through topotactic transformation of $MnCO_3$. *Nanoscale* **2013**, *5*, 2352−2357.
(35) He, Y.; Feng, Q.; Zhang, S. Q.; Zou, Q. L.; Wu, X. L.; Yang, X. J. Strategy for Lowering Li Source Dosage While Keeping High Reactivity in Solvothermal Synthesis of $LiMnO_2$ Nanocrystals. *ACS Sustainable Chem. Eng.* **2013**, *1*, 570−573.
(36) Jang, Y.; Chiang, Y. M. Stability of the monoclinic and orthorhombic phases of $LiMnO_2$ with temperature, oxygen partial pressure, and Al doping. *Solid State Ionics* **2000**, *130*, 53−59.
(37) Thackeray, M. M.; Kang, S. H.; Johnson, C. S.; Vaughey, J. T.; Benedeka, R.; Hackney, S. A. Li_2MnO_3-stabilized $LiMO_2$ (M = Mn, Ni, Co) electrodes for lithium-ion batteries. *J. Mater. Chem.* **2007**, *17*, 3112−3125.
(38) Ohzuku, T.; Kitagawa, M.; Hirai, T. Electrochemistry of manganese dioxide in lithium nonaqueous Cell: III. X-Ray diffractional study on the reduction of spinel-related manganese dioxide. *J. Electrochem. Soc.* **1990**, *137* (3), 769−775.
(39) Huang, X. K.; Zhang, Q. S.; Chang, H. T.; Gan, J. L.; Yue, H. J.; Yang, Y. Hydrothermal Synthesis of Nanosized $LiMnO_2$ - Li_2MnO_3 compounds and their electrochemical performances. *J. Electrochem. Soc.* **2009**, *156* (3), A162−A168.